Enhancing accuracy with subpixel smoothing for multiband effective-mass Hamiltonians of semiconductor nanostructures

Chi-Ti Hsieh[a], Tung-Han Hsieh[a], and Shu-Wei Chang[a,b]

[a]Research Center for Applied Sciences, Academia Sinica, Nankang, Taipei 11529, Taiwan
[b]Department of Photonics, National Chiao-Tung University, Hsinchu 30010, Taiwan

ABSTRACT

The spatial discontinuity of physical parameters at an abrupt interface may increase numerical errors when solving partial differential equations. Rather than generating boundary-adapted meshes for objects with complicated geometry in the finite-element method, the subpixel smoothing (SPS) replaces discontinuous parameters inside square elements that are bisected by interfaces in, for example, the finite-difference (FD) method, with homogeneous counterparts and matches physical boundary conditions therein. In this work, we apply the idea of SPS to the eight-band effective-mass Luttinger-Kohn (LK) and Burt-Foreman (BF) Hamiltonians of semiconductor nanostructures. Two smoothing approaches are proposed. One stems from eliminations of the first-order perturbation in energy, and the other is an application of the Hellmann-Feynman (HF) theorem. We employ the FD method to numerically solve the eigenvalue problem corresponding to the multiband Schrodinger's equation for circular quantum wires (QWRs). The eigenenergies and envelope (wave) functions for valence and conduction states in III-V circular QWRs are examined. We find that while the procedure of perturbation theory seems to have the better accuracy than that of HF theorem, the errors of both schemes are considerably lower than that without smoothing or with direct but unjustified averages of parameters. On the other hand, even in the presence of SPS, the numerical results for the LK Hamiltonian of nanostructures could still contain nonphysical spurious solutions with extremely localized states near heterostructure interfaces. The proper operator ordering embedded in the BF Hamiltonian mitigates this problem. The proposed approaches may improve numerical accuracies and reduce computational cost for the modeling of nanostructures in optoelectronic devices.

Keywords: Subpixel smoothing, multiband $k \cdot p$ method, first-order perturbation, Hellmann-Feynman theorem, quantum wires

1. INTRODUCTION

The discontinuity of physical parameters at an abrupt interface is a known source of errors in numerical solutions to partial differential equations. For the finite-difference (FD) method, with spatially smooth parameters and proper approximations of the first- and second-order derivatives, the numerical errors scale as $O(N^{-2})$, where N is the number of grid points along one dimension. However, the discontinuity often increases the errors over this level and enhances the computational cost to reach a given level of accuracies. Hence, the treatments for spatial discontinuities may be necessary when numerically solving partial differential equations.

The treatment of the spatial discontinuity is often implemented prior to computations, for example, generations of boundary-adapted meshes in the finite-element method. Rather than adapting computation grids to the complex geometry of objects, the subpixel smoothing (SPS) replaces discontinuous parameters inside an interface-bisected element with locally homogeneous counterparts, which eliminate errors perturbatively but respect the physical BCs there. The further usage of simple Cartesian grids in the FD method eases many calculations afterwards. In this way, the computational accuracy may be improved without significantly altering the intuitive implementation of the FD method. In fact, these concepts have been utilized to compute Maxwell's equations in electromagnetism for reductions of the errors caused by the discontinuities to the second

Further author information: (Send correspondence to Shu-Wei Chang)
Chi-Ti Hsieh: E-mail: ch2hsieh@sinica.edu.tw
Tung-Han Hsieh: E-mail: thhsieh@sinica.edu.tw
Shu-Wei Chang: E-mail: swchang@sinica.edu.tw

Physics and Simulation of Optoelectronic Devices XXIV, edited by
Bernd Witzigmann, Marek Osiński, Yasuhiko Arakawa, Proc. of SPIE Vol. 9742,
97421M · © 2016 SPIE · CCC code: 0277-786X/16/$18 · doi: 10.1117/12.2211679

order in isotropic[1,2] and anisotropic media.[3,4] The SPS algorithm is also built into software package MEEP for computations in optics and electromagnetism.[5]

In this paper, we generalize the concept of SPS to the calculations of envelope (wave) functions in semiconductor nanostructures to enhance the accuracy of FD computations. The partial differential equations originate from the multiband Hamiltonian operators of semiconductors under the effective-mass approximation ($k \cdot p$ method). For example, the eight-band Luttinger-Kohn (LK) Hamiltonian[6] corrected by Bir-Pikus (BP) strain terms[7] gives a useful technique for the modeling of semiconductor bulks and nanostructures.[8,9] The numerical results of this Hamiltonian, however, occasionally contain two types of nonphysical spurious solutions:[10] (1) wing-band solutions which exhibit highly oscillatory patterns and energies located in the bandgap due to inadequate material parameters,[11–13] and (2) extremely localized solutions near interfaces of heterostructure.[14,15] The proper operator ordering provided by Burt and Foreman (BF)[16–18] could remove this problem[14,15] and has been implemented in the four- and six-band valence Hamiltonians.[19,20] We note, on the other hand, that the SPS schemes only improve the numerical accuracy but cannot eliminate the spurious solutions.

The proposed SPS schemes for the effective-mass Hamiltonians are based on the continuity of envelop functions and effective probability flux densities normal to interfaces. The idea is to express the deviation in energy (or its variations with some external variables) with the substitution of unknown smoothed parameters in terms of *continuous* fields and associated *transformed* parameters. The discontinuity is included in those transformed parameters, and one can average them while demanding the deviation to vanish. The smoothed parameters are then calculated in the condition of vanishing deviations. If the target is the energy, the SPS procedure is similar to eliminations of the first-order energy change in the perturbation theory (PT). Alternatively, if energy variations with external variables are considered, the scheme is given in the form of Hellmann-Feynman (HF) theorem.[1,3] We will use the FD method to demonstrate the SPS schemes for circular quantum wires (QWRs). The numerical errors of two SPS schemes are lower than that without smoothing or with direct averages of original parameters.

The remaining context of the paper is organized below. In Section 2, we introduce the general form of multiband Hamiltonian operator of nanostructures for eigenenergy and envelop-function computations. In Section 3, we first describe the concepts of SPS using the grid points for FD calculations. Two SPS procedures based on the elimination of energy perturbations and HF theorem are then expressed. In Section 4, based on the eight-band BF Hamiltonian, we calculate relative errors in eigenenergies of circular QWRs with two developed SPS schemes. These errors will be compared to those without smoothing and with direct averages (DA) of untransformed parameters. A conclusion is presented in Section 5, and details of the formulation will be given in the appendix.

2. MULTIBAND EFFECTIVE-MASS HAMILTONIAN

The multiband effective-mass Hamiltonian based on $k \cdot p$ method is a useful technique for bandstructure computations of bulk semiconductors near the Brillouin zone (BZ) center. In the eight-band spaces, two conduction (C) and six valence bands are included. The six valence bands contain two heavy-hole (HH), two light-hole (LH), and two spin-orbit split-off (SO) bands. Because of Lowdin's perturbations from remote ones other than these eight bands, the bulk Hamiltonian includes second-order corrections of the real wave vector $\mathbf{k}$.[8] In Appendix A, we present matrix elements $H_{jj'}[\mathbf{k}]$ ($j, j' = 1-8$ are band indices) of the eight-band BF Hamiltonian of semiconductor nanostructures. The eight-band LK counterpart could be treated as a special case of the BF Hamiltonian and is only briefly discussed there. The band labels and Bloch parts are listed in Table 3 in the same appendix.

The matrix element $H_{jj'}[\mathbf{k}]$ of the multiband effective Hamiltonian of bulk semiconductors could be presented in Cartesian components (k_x, k_y, k_z) of wave vector $\mathbf{k}$ as[21] (x, y, z axes are aligned with main crystal axes)

$$H_{jj'}[\mathbf{k}] = \sum_{\alpha,\beta} k_\alpha D^{\alpha\beta}_{jj'} k_\beta + \frac{1}{2}\sum_{\alpha}\left(k_\alpha T^{\alpha}_{jj'} + T^{\ddagger\alpha}_{jj'} k_\alpha\right) + W_{jj'}, \quad W_{jj'} = V_j \delta_{jj'} + H^{(\mathrm{BP})}_{jj'}, \tag{1}$$

where superscripts α, β indicate indices x, y, z; $D^{\alpha\beta}_{jj'}$ and $T^{\alpha}_{jj'}$ (and $T^{\ddagger\alpha}_{jj'}$) are material parameters associated with the quadratic and linear terms of $\mathbf{k}$, respectively; symbol $\ddagger$ denotes a hermitian conjugate (h.c.) to be explained

below; $W_{jj'}$ is a matrix which is hermitian in indices j, j'; V_j indicates the unstrained energy of band j at the BZ center; $\delta_{jj'}$ is the Kronecker delta; and $H^{(\mathrm{BP})}_{jj'}$ is a hermitian matrix which includes the BP strain terms.[8,9] In the eight-band scheme, parameter $D^{\alpha\beta}_{jj'}$ contain the modified inverse effective mass γ_c in conduction bands and three modified Luttinger parameters γ_1, γ_2, and γ_3 in valence bands, and $T^{\alpha}_{jj'}$ and $T^{\ddagger\alpha}_{jj'}$ are proportional to the interband momentum matrix element P_{cv}.

There are two sets of indices $j, j' \in \{1-8\}$ and $\alpha, \beta \in \{x, y, z\}$ in parameters $D^{\alpha\beta}_{jj'}$ and $T^{\alpha}_{jj'}$ ($T^{\ddagger\alpha}_{jj'}$). We denote the symbol "T" for the transposition in indices α, β:

$$D^{\mathrm{T}\alpha\beta}_{jj'} = [\mathbf{D}^{\mathrm{T}}_{jj'}]^{\alpha\beta} \equiv D^{\beta\alpha}_{jj'} = [\mathbf{D}_{jj'}]^{\beta\alpha}, \quad T^{\mathrm{T}\alpha}_{jj'} = [\mathbf{T}^{\mathrm{T}}_{jj'}]^{\mathbf{1},\alpha} \equiv T^{\alpha}_{jj'} = [\mathbf{T}_{jj'}]^{\alpha,\mathbf{1}}, \tag{2}$$

where $\mathbf{D}_{jj'}$ and $\mathbf{D}^{\mathrm{T}}_{jj'}$ are space tensors including matrix elements $D^{\alpha\beta}_{jj'}$; $\mathbf{T}_{jj'}$ and $\mathbf{T}^{\mathrm{T}}_{jj'}$ indicate *column* and *row* vectors composed of $T^{\alpha}_{jj'}$, respectively; and $\mathbf{1}$ is a column/row index of unity size. In order to avoid the confusion with notation † which is conventionally reserved for the conjunction of transposition "T" and complex conjugation "$*$", we adopt an another symbol ‡ for the hermitian conjugation related to band indices j, j':

$$D^{\ddagger\alpha\beta}_{jj'} \equiv D^{\alpha\beta *}_{j'j}, \quad T^{\ddagger\alpha}_{jj'} \equiv T^{\alpha *}_{j'j}. \tag{3}$$

For nanostructures, the Hamiltonian matrix element $H_{jj'}[\mathbf{k}]$ contains the dependency on position $\mathbf{r}$, and k_α is replaced by $-i\partial/\partial\alpha \equiv -i\partial_\alpha$. From Ref. 21, we have the condition

$$D^{\ddagger\alpha\beta}_{jj'} \equiv D^{\alpha\beta *}_{j'j} = D^{\beta\alpha}_{jj'} \ \ (\text{not } D^{\alpha\beta}_{jj'}), \tag{4}$$

indicating that $D^{\alpha\beta}_{jj'}$ need not be hermitian in j, j'. Rewriting Eq. (4) as $D^{(\mathrm{T}\ddagger)\alpha\beta}_{jj'} = D^{\alpha\beta}_{jj'}$ shows that $D^{\alpha\beta}_{jj'}$ is hermitian in joint indices (α, j) and (β, j'). The BF and LK Hamiltonian operators both satisfy Eq. (4). The LK Hamiltonian has another hermiticity $D^{\ddagger\alpha\beta}_{jj'} = D^{\alpha\beta}_{jj'}$ in indices j, j' and symmetry $D^{\mathrm{T}\alpha\beta}_{jj'} = D^{\alpha\beta}_{jj'}$ in indices α, β. However, only the matrix condition in Eq. (4) has to be preserved in SPS schemes. We note that the simultaneous presences of $T^{\alpha}_{jj'}$ and $T^{\ddagger\alpha}_{jj'}$ which are h.c. to each other in Eq. (1) hold the hermiticity of the Hamiltonian operator.

For dimensionless computation, we define the normalized parameters with a length scale L_{nor} and normalization energy $E_{\mathrm{nor}} = \hbar^2/(2m_0 L^2_{\mathrm{nor}})$, where $\hbar$ is Planck's constant divided by 2π, and m_0 is the free-electron mass, as below:

$$q_\alpha = k_\alpha L_{\mathrm{nor}}, \quad \Gamma^{\alpha\beta}_{jj'} = \frac{D^{\alpha\beta}_{jj'}}{L^2_{\mathrm{nor}} E_{\mathrm{nor}}}, \quad \Lambda^{\alpha}_{jj'} = \frac{T^{\alpha}_{jj'}}{2L_{\mathrm{nor}} E_{\mathrm{nor}}}, \quad \tilde{W}_{jj'} = \frac{W_{jj'}}{E_{\mathrm{nor}}}, \quad \tilde{V}_j = \frac{V_j}{E_{\mathrm{nor}}}, \quad \tilde{H}^{(\mathrm{BP})}_{jj'} = \frac{H^{(\mathrm{BP})}_{jj'}}{E_{\mathrm{nor}}}. \tag{5}$$

The unit-free Hamiltonian matrix element $\tilde{H}_{jj'}[\mathbf{q}] \equiv H_{jj'}[\mathbf{k}]/E_{\mathrm{nor}}$ is described as

$$\tilde{H}_{jj'}[\mathbf{q}] = \sum_{\alpha,\beta} q_\alpha \Gamma^{\alpha\beta}_{jj'} q_\beta + \sum_{\alpha} \left(q_\alpha \Lambda^{\alpha}_{jj'} + \Lambda^{\ddagger\alpha}_{jj'} q_\alpha \right) + \tilde{W}_{jj'}, \tag{6}$$

where q_α is a dimensionless differential operator $q_\alpha \to -iL_{\mathrm{nor}}\partial_\alpha$ in the real space. For QWRs, we indicate the z axis as the wire axis and rewrite the matrix element $\tilde{H}_{jj'}[\mathbf{q}]$ with new normalized parameters for QWRs (subscripted with "wr") as

$$\begin{aligned} \tilde{H}_{jj'}[\mathbf{q}] &= \sum_{\alpha,\beta=x,y} q_\alpha \Gamma^{\alpha\beta}_{jj'} q_\beta + \sum_{\alpha=x,y} \left[q_\alpha \Lambda^{\alpha}_{\mathrm{wr},jj'}(k_z) + \Lambda^{\ddagger\alpha}_{\mathrm{wr},jj'}(k_z) q_\alpha \right] + \tilde{W}_{\mathrm{wr},jj'}(k_z), \\ \Lambda^{\alpha}_{\mathrm{wr},jj'}(k_z) &= \Lambda^{\alpha}_{jj'} + \Gamma^{\alpha z}_{jj'} q_z, \ \forall\ \alpha = x, y, \quad \tilde{W}_{\mathrm{wr},jj'}(k_z) = \tilde{W}_{jj'} + q_z^2 \Gamma^{zz}_{jj'} + q_z(\Lambda^{z}_{jj'} + \Lambda^{\ddagger z}_{jj'}), \end{aligned} \tag{7}$$

where the wave number k_z is a label for QWR states.

For nanostructures, the dependency on position $\mathbf{r}$ appears in parameters $D^{\alpha\beta}_{jj'}(\mathbf{r})$, $T^{\alpha}_{jj'}(\mathbf{r})$, $W_{jj'}(\mathbf{r})$, and $V_j(\mathbf{r})$ in Eq. (1), and normalized ones $\Gamma^{\alpha\beta}_{jj'}(\mathbf{r})$, $\Lambda^{\alpha}_{jj'}(\mathbf{r})$, $\tilde{W}_{jj'}(\mathbf{r})$, and $\tilde{V}_j(\mathbf{r})$ in Eq. (6). The wave function $\Psi^{(n)}(\mathbf{r})$ of state $|n\rangle$ and associated Schrodinger's equation in an inhomogeneous space are given as

$$\Psi^{(n)}(\mathbf{r}) = \sum_j \psi^{(n)}_j(\mathbf{r}) u_j(\mathbf{r}), \qquad \sum_{j'} H_{jj'}\left[\mathbf{k} = -i\nabla, \mathbf{r}\right] \psi^{(n)}_{j'}(\mathbf{r}) = E_n \psi^{(n)}_j(\mathbf{r}), \tag{8}$$

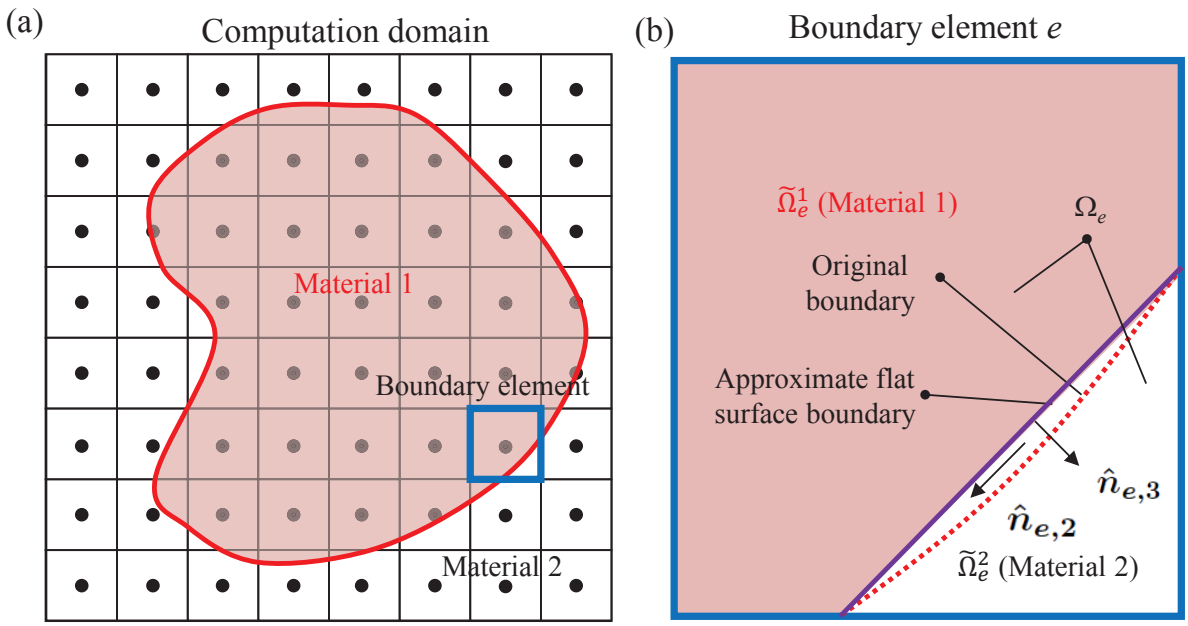

Figure 1. (a) The 2D computation domain discretized by the square grid points (black circles). The QWR is composed of material 1, and the region outside it is made up of material 2. The grids are located at the centers of pixels. A boundary element e is circumscribe in blue. (b) Details of element e. The purple line is the approximate flat boundary which replaces the original curved one (red dots). This new boundary divides Ω_e into $\tilde{\Omega}_e^1$ (material 1) and $\tilde{\Omega}_e^2$ (material 2). Unit vector $\hat{n}_{e,3}$ is the surface norm of the new boundary while $\hat{n}_{e,1}$ (pointing out of paper) and $\hat{n}_{e,2}$ are tangential ones.

where $\psi_j^{(n)}(\mathbf{r})$ and $u_j(\mathbf{r})$ are the envelope function and position representation of Bloch part $|u_j\rangle$ for band j, respectively; $\mathbf{k}$ is replaced with the differential operator $-i\nabla$; and E_n is the eigenenergy of state $|n\rangle$. For QWRs, we rewrite the wave function $\Psi^{(n,k_z)}(\mathbf{r})$, and Schrodinger's equation of state $|n,k_z\rangle$ are given as

$$\Psi^{(n,k_z)}(\mathbf{r}) = \frac{e^{ik_z z}}{\sqrt{L_{\rm wr}}} \sum_j \psi_j^{(n,k_z)}(\boldsymbol{\rho}) u_j(\mathbf{r}), \quad \sum_{j'} H_{jj'}[k_{x,y} = -i\partial_{x,y}, k_z, \boldsymbol{\rho}] \psi_{j'}^{(n,k_z)}(\boldsymbol{\rho}) = E_{n,k_z} \psi_j^{(n,k_z)}(\boldsymbol{\rho}), \tag{9}$$

where index n is now the subband label; $L_{\rm wr}$ is the length of the QWR; $\boldsymbol{\rho} = x\hat{x} + y\hat{y}$ is the transverse coordinate; $\psi_j^{(n,k_z)}(\boldsymbol{\rho})$ is the component of envelop functions aside to the phase factor $\exp(ik_z z)$; and E_{n,k_z} is the eigenenergy of state $|n,k_z\rangle$.

The multiband Schrodinger's equations in Eqs. (8) and (9) are presented as the eigenvalue problems. We will implement the FD method[22,23] to solve eigenenergies E_{n,k_z} and envelop functions $\psi_j^{(n,k_z)}(\boldsymbol{\rho})$ of states in circular QWRs. Moreover, if the anisotropy on the xy plane is small, the axial approximation will be utilized.[8,24]

3. SUBPIXEL SMOOTHING IN MULTIBAND HAMILTONIANS

In Fig. 1(a), the two-dimensional (2D) computation domain of the cross section of a QWR is discretized by square mesh grids (black circles), on which the values of material parameters are assigned. The grid points for FD calculations are located at centers of square elements (pixels). The wire extends out of Fig. 1(a). Its boundary (red curve) is a surface. The regions inside and outside the boundary are made up of materials 1 and 2, respectively. In Fig. 1(a), a boundary element e is circumscribed in blue, and its detail is plotted in Fig. 1(b). Since the element is small, the true boundary surface (red curved dots) can be approximated as a flat surface (purple straight line) locally. This surface divides element area Ω_e into two regions $\tilde{\Omega}_e^1$ (material 1) and $\tilde{\Omega}_e^2$ (material 2). The local flat surface has a unit surface norm $\hat{n}_{e,3}$ and two tangential unit vectors $\hat{n}_{e,1}$ and $\hat{n}_{e,2}$. We assign the vector $\hat{n}_{e,1}$ parallel to the QWR axis (pointing out of the paper) as $\hat{z}$. The three unit vectors $\hat{n}_{e,w}$ $(w = 1-3)$ form a right-hand coordinate system.

From SPS procedures, we replace the inhomogeneous material parameters in boundary elements with homogeneous counterparts which are set to grid points. The continuity condition across the boundary has to be considered.[1,3] In the following context, we will neglect the state symbol n of envelop functions. In a boundary element e, both (1) the envelope functions $\psi_j(\mathbf{r})$ at two sides of the interface and (2) their effective probability flux density normal to the interface have to be continuous. They are related to the BCs of gradient fields defined as $\mathbf{K}_j(\mathbf{r}) \equiv \mathbf{q}\psi_j(\mathbf{r}) \to -iL_{\rm nor}\nabla\psi_j(\mathbf{r})$. The expression of the effective probability flux density based on Eq. (1) can be found in Ref. 21. From there, condition (2) is equivalent to the requirement that a vector field $\boldsymbol{\eta}_j(\mathbf{r})$, which is related to the probability flux density and defined as

$$\boldsymbol{\eta}_j(\mathbf{r}) = \sum_{j'} \left[\boldsymbol{\Gamma}_{jj'}(\mathbf{r})\mathbf{K}_{j'}(\mathbf{r}) + \boldsymbol{\Lambda}_{jj'}(\mathbf{r})\psi_{j'}(\mathbf{r})\right], \tag{10}$$

has a continuous normal component across the interface. In boundary element e, the normal component $\eta_j^{(3)}(\mathbf{r})$ is given as

$$\eta_j^{(3)}(\mathbf{r}) = \hat{n}_{e,3}\cdot\boldsymbol{\eta}_j(\mathbf{r}) = \sum_{j'}\left[\Gamma_{jj'}^{(33)}(\mathbf{r})K_{j'}^{(3)}(\mathbf{r}) + \boldsymbol{\Gamma}_{jj'}^{(3t)}(\mathbf{r})\mathbf{K}_{j'}^{(t)}(\mathbf{r}) + \Lambda_{jj'}^{(3)}(\mathbf{r})\psi_{j'}(\mathbf{r})\right], \tag{11}$$

where symbols t and 3 denote the tangential and normal directions to the interface, respectively. Using this relation, we present the discontinuous field $K_j^{(3)}(\mathbf{r})$ with other continuous fields as

$$K_j^{(3)}(\mathbf{r}) = \sum_h \Xi_{jh}(\mathbf{r})\eta_h^{(3)}(\mathbf{r}) - \sum_{h,l}\Xi_{jh}(\mathbf{r})\boldsymbol{\Gamma}_{hl}^{(3t)}(\mathbf{r})\mathbf{K}_l^{(t)}(\mathbf{r}) - \sum_{h,l}\Xi_{jh}(\mathbf{r})\Lambda_{hl}^{(3)}(\mathbf{r})\psi_l(\mathbf{r}), \quad \Xi_{jj'}(\mathbf{r}) \equiv \left[\Gamma^{(33)}(\mathbf{r})\right]_{jj'}^{-1}, \tag{12}$$

where $\Xi_{jj'}(\mathbf{r})$ is the inverse of $\Gamma_{jj'}^{(33)}(\mathbf{r})$ in the eight-band space.

With the normalization of envelope functions to unity, the normalized energy $\tilde{E} \equiv E/E_{\rm nor}$ is presented as

$$\begin{aligned}\tilde{E} &= \sum_{j,j'}\int \mathrm{d}\mathbf{r}\psi_j^*(\mathbf{r})\tilde{H}_{jj'}[\mathbf{k} = -i\nabla, \mathbf{r}]\psi_{j'}(\mathbf{r}) \\ &= \sum_{j,j'}\int \mathrm{d}\mathbf{r}\left[\mathbf{K}_j^\dagger(\mathbf{r})\boldsymbol{\Gamma}_{jj'}(\mathbf{r})\mathbf{K}_{j'}(\mathbf{r}) + \mathbf{K}_j^\dagger(\mathbf{r})\boldsymbol{\Lambda}_{jj'}(\mathbf{r})\psi_{j'}(\mathbf{r}) + \psi_j^*(\mathbf{r})\boldsymbol{\Lambda}_{jj'}^{(\mathrm{T}\ddagger)}(\mathbf{r})\mathbf{K}_{j'}(\mathbf{r}) + \psi_j^*(\mathbf{r})\tilde{W}_{jj'}(\mathbf{r})\psi_{j'}(\mathbf{r})\right],\end{aligned} \tag{13}$$

where the operation $\mathbf{a}^\dagger\mathbf{b}$ between column vectors $\mathbf{a}$ and $\mathbf{b}$ indicates $\mathbf{a}^*\cdot\mathbf{b}$. The integrand in Eq. (13) represents quadratic terms of envelop functions $\psi_j(\mathbf{r})$, gradient fields $\mathbf{K}_j(\mathbf{r})$, and their complex conjugates (c.c.). We may rewrite the normalized energy $\tilde{E}$ in the general form as

$$\tilde{E} = \sum_{j,j'}\int \mathrm{d}\mathbf{r}\left[\sum_p f_{p,j}^*(\mathbf{r})\lambda_{p,jj'}(\mathbf{r})g_{p,j'}(\mathbf{r})\right], \tag{14}$$

where p is the label of parameters in the set $\{\boldsymbol{\Gamma}_{jj'}(\mathbf{r}),\ \boldsymbol{\Lambda}_{jj'}(\mathbf{r}),\ \boldsymbol{\Lambda}_{jj'}^{(\mathrm{T}\ddagger)}(\mathbf{r}),\ \tilde{W}_{jj'}(\mathbf{r})\}$; $\lambda_{p,jj'}(\mathbf{r})$ is the parameter corresponding to p; and $f_{p,j}^*(\mathbf{r})$ and $g_{p,j'}(\mathbf{r})$ are fields associated with $\lambda_{p,jj'}(\mathbf{r})$, which include $\{\psi_j^*(\mathbf{r}), \mathbf{K}_j^\dagger(\mathbf{r})\}$ and $\{\psi_{j'}(\mathbf{r}), \mathbf{K}_{j'}(\mathbf{r})\}$, respectively. Equations (13) and (14) are utilized to calculate the smoothed parameters in boundary elements.

3.1 Subpixel smoothing based on perturbation theory

We first study the first-order perturbation in normalized energy for the smoothing of material parameters in boundary elements e. The smoothed parameters $\boldsymbol{\Gamma}_{e,jj'}^{\rm PT}$, $\boldsymbol{\Lambda}_{e,jj'}^{\rm PT}$, and $\tilde{W}_{e,jj'}^{\rm PT}$ in the PT scheme are different from heterogeneous ones $\boldsymbol{\Gamma}_{jj'}(\mathbf{r})$, $\boldsymbol{\Lambda}_{jj'}(\mathbf{r})$, and $\tilde{W}_{jj'}(\mathbf{r})$ there. The deviations are

$$\Delta\boldsymbol{\Gamma}_{jj'}(\mathbf{r}) = \boldsymbol{\Gamma}_{e,jj'}^{\rm PT} - \boldsymbol{\Gamma}_{jj'}(\mathbf{r}), \quad \Delta\boldsymbol{\Lambda}_{jj'}(\mathbf{r}) = \boldsymbol{\Lambda}_{e,jj'}^{\rm PT} - \boldsymbol{\Lambda}_{jj'}(\mathbf{r}), \quad \Delta\tilde{W}_{jj'}(\mathbf{r}) = \tilde{W}_{e,jj'}^{\rm PT} - \tilde{W}_{jj'}(\mathbf{r}). \tag{15}$$

The first-order perturbation $\Delta\tilde{E}^{(1)}$ in $\tilde{E}$ due to these parameter deviations is described as

$$\Delta\tilde{E}^{(1)} = \sum_{e}\sum_{j,j'}\left\{\int_{\Omega_e} \mathrm{d}\mathbf{r}\left[\sum_{p} f^{*}_{p,j}(\mathbf{r})\lambda^{\mathrm{PT}}_{e,p,jj'}g_{p,j'}(\mathbf{r})\right] - \int_{\Omega_e} \mathrm{d}\mathbf{r}\left[\sum_{p} f^{*}_{p,j}(\mathbf{r})\lambda_{p,jj'}(\mathbf{r})g_{p,j'}(\mathbf{r})\right]\right\}, \tag{16}$$

where a smoothed parameter $\lambda^{\mathrm{PT}}_{e,p,jj'}$ belongs to the set $\{\mathbf{\Gamma}^{\mathrm{PT}}_{e,jj'}, \mathbf{\Lambda}^{\mathrm{PT}}_{e,jj'}, \mathbf{\Lambda}^{\mathrm{PT(T\ddagger)}}_{e,jj'}, \tilde{W}^{\mathrm{PT}}_{e,jj'}\}$ of boundary element e.

In boundary element e, we substitute the material tensors referenced to $\hat{n}_{e,w}$ ($w = 1{-}3$) and tangential/normal components $\mathbf{K}^{(t)}_{j}(\mathbf{r})/K^{(3)}_{j}(\mathbf{r})$ of the gradient field $\mathbf{K}_j(\mathbf{r})$ into the perturbation $\Delta\tilde{E}^{(1)}$. The substitutions are related to a transformation from the Cartesian coordinate to local one in element e. We then substitutes the discontinuous field $K^{(3)}_{j}(\mathbf{r})$ with the continuous one $\eta^{(3)}_{j}(\mathbf{r})$ through Eq. (12). The new integrand still maintains a quadratic form in terms of $\psi_j(\mathbf{r})$, $\mathbf{K}^{(t)}_{j}(\mathbf{r})$, and $\eta^{(3)}_{j}(\mathbf{r})$. The detail of derivations is shown in Ref. 21. In brief, the generic form of $\Delta\tilde{E}^{(1)}$ is presented as

$$\begin{aligned}
\Delta\tilde{E}^{(1)} &= \sum_{e}\sum_{j,j'} V_e\langle\Delta I^{\mathrm{PT}}_{e,jj'}(\mathbf{r})\rangle_e, \quad \langle\Delta I^{\mathrm{PT}}_{e,jj'}(\mathbf{r})\rangle_e \equiv \frac{1}{V_e}\int_{\Omega_e}\mathrm{d}\mathbf{r}\Delta I^{\mathrm{PT}}_{e,jj'}(\mathbf{r}),\\
\Delta I^{\mathrm{PT}}_{e,jj'}(\mathbf{r}) &= \sum_{s} F^{*}_{s,j}(\mathbf{r})\Big[\kappa_{e,s,jj'}\{\lambda^{\mathrm{PT}}_{e,p,ll'}, \lambda_{a,hh'}(\mathbf{r})\} - \kappa_{s,jj'}\{\lambda_{p,ll'}(\mathbf{r})\}\Big]G_{s,j'}(\mathbf{r}),
\end{aligned} \tag{17}$$

where $\Delta I^{\mathrm{PT}}_{e,jj'}(\mathbf{r})$ is the integrand corresponds to parameter deviations; $\langle\ldots\rangle_e$ is the average in region Ω_e with volume V_e; s is the label of transformed parameters; $F^{*}_{s,j}(\mathbf{r})$ and $G_{s,j'}(\mathbf{r})$ include sets of continuous fields $\{\psi^{*}_{j}(\mathbf{r}), \mathbf{K}^{\dagger(t)}_{j}(\mathbf{r}), \eta^{(3)*}_{j}(\mathbf{r})\}$ and $\{\psi_{j'}(\mathbf{r}), \mathbf{K}^{(t)}_{j'}(\mathbf{r}), \eta^{(3)}_{j'}(\mathbf{r})\}$, respectively; $\kappa_{e,s,jj'}\{\lambda^{\mathrm{PT}}_{e,p,ll'}, \lambda_{a,hh'}(\mathbf{r})\}$ is the effective parameter transformed from original smoothed parameters $\lambda^{\mathrm{PT}}_{e,p,ll'}$; and $\kappa_{s,jj'}\{\lambda_{p,ll'}(\mathbf{r})\}$ is the counterpart transformed from $\lambda_{p,ll'}(\mathbf{r})$.

As element e is small enough, the continuous fields $F^{*}_{s,j}(\mathbf{r})$ and $G_{s,j'}(\mathbf{r})$ do not vary much within Ω_e, and we can factor them out of the volume integral in Eq. (17) so that the volume average is only applied to the discontinuous transformed parameters. To eliminate the first-order perturbation $\Delta\tilde{E}^{(1)}$, the averages of parameter deviations in Eq. (17) are required to vanish term by term for each parameter label s:

$$\langle\kappa_{e,s,jj'}\{\lambda^{\mathrm{PT}}_{e,p,ll'}, \lambda_{a,hh'}(\mathbf{r})\}\rangle_e = \langle\kappa_{s,jj'}\{\lambda_{p,ll'}(\mathbf{r})\}\rangle_e, \tag{18}$$

Equation (18) stands for a set of linear equations for smoothed parameters $\lambda^{\mathrm{PT}}_{e,p,ll'}$, which could be calculated self-consistently with the procedures provided in Ref. 21.

3.2 Subpixel smoothing based on Hellmann-Feynman theorem

Assume that material parameters $\mathbf{\Gamma}_{jj'}(\mathbf{r})$, $\mathbf{\Lambda}_{jj'}(\mathbf{r})$, and $\tilde{W}_{jj'}(\mathbf{r})$ are parameterized by a set of external variables $\{\nu_M\}$. Both the envelop functions $\psi_j(\mathbf{r})$ and gradient fields $\mathbf{K}_j(\mathbf{r})$ depend on $\{\nu_M\}$ implicitly from Eq. (8). For a variable ν^{e}_{m} in the subset $\{\nu_M\}$ associated with boundary element e, the HF theorem indicates that the variation of the normalized energy $\tilde{E}$ with ν^{e}_{m} is[25]

$$\frac{\partial\tilde{E}}{\partial\nu^{e}_{m}} \equiv \sum_{j,j'}\int_{\Omega_e}\mathrm{d}\mathbf{r}I^{\mathrm{HF}}_{e,jj'}(\mathbf{r}) = \sum_{j,j'} V_e\langle I^{\mathrm{HF}}_{e,jj'}(\mathbf{r})\rangle_e, \quad I^{\mathrm{HF}}_{e,jj'}(\mathbf{r}) = \sum_{p} f^{*}_{p,j}(\mathbf{r})\frac{\partial\lambda_{p,jj'}(\mathbf{r})}{\partial\nu^{e}_{m}}g_{p,j'}(\mathbf{r}), \tag{19}$$

where $I^{\mathrm{HF}}_{e,jj'}(\mathbf{r})$ is the associated integrand. With similar procedures in Section 3.1, the substitution of $K^{(3)}_{j}(\mathbf{r})$ with $\eta^{(3)}_{j}(\mathbf{r})$ transforms the integrand $I^{\mathrm{HF}}_{e,jj'}(\mathbf{r})$ into

$$I^{\mathrm{HF}}_{e,jj'}(\mathbf{r}) = \sum_{s} F^{*}_{s,j}(\mathbf{r})\kappa_{e,s,jj'}\left\{\frac{\partial\lambda_{p,ll'}(\mathbf{r})}{\partial\nu^{e}_{m}}, \lambda_{a,hh'}(\mathbf{r})\right\}G_{s,j'}(\mathbf{r}), \tag{20}$$

Table 1. Material parameters in eight-band calculations[8,26]

Parameter	Symbol (unit)	GaAs	InAs	InP	GaP
Lattice constant	a (Å)	5.6533	6.0584	5.8688	5.4505
Bandgap energy at 300K	E_g (eV)	1.424	0.354	1.344	2.78
Spin-orbit split-off energy	Δ (eV)	0.34	0.38	0.11	0.08
Deformation potential	a_v (eV)	1.16	1.00	1.27	1.70
Optical matrix parameter	E_p (eV)	25.7	22.2	20.7	22.2
Modified optical matrix parameter	E_p' (eV)	21.36	18.17	16.53	13.70
Average energy of three valence bands	$E_{v,av}$ (eV)	-6.92	-6.67	-7.04	-7.40
Relative conduction effective mass	m_c (m_0)	0.0665	0.023	0.077	0.17
Luttinger parameters[26]	γ_1^{L}	7.65	19.67	6.28	4.20
	γ_2^{L}	2.41	8.37	2.08	0.98
	γ_3^{L}	3.28	9.29	2.76	1.66
	κ^{L}	1.72	7.68	1.47	0.34
Inverse of modified relative conduction effective mass[15]	γ_c	1.0	1.0	1.0	1.0
Modified Luttinger parameters	γ_1	3.018	7.067	2.290	2.573
	γ_2	0.094	2.069	0.085	0.166
	γ_3	0.964	2.989	0.765	0.846
	κ	-0.596	1.379	-0.525	-0.474

Table 2. Material parameters in compound $Ga_{0.18}In_{0.82}As_{0.4}P_{0.6}$

E_g (eV)	γ_1	γ_2	γ_3	κ
1.058	3.934	0.742	1.515	0.097

where the functional forms of the transformed parameters $\kappa_{e,s,jj'}\{\ldots\}$ in Eq. (17) show up here. One can show

$$I^{\mathrm{HF}}_{e,jj'}(\mathbf{r}) = \sum_s F^*_{s,j}(\mathbf{r}) \frac{\partial \tau_{s,jj'}\{\lambda_{p,ll'}(\mathbf{r})\}}{\partial \nu^e_m} G_{s,j'}(\mathbf{r}), \quad \frac{\partial \tau_{s,jj'}\{\lambda_{p,ll'}(\mathbf{r})\}}{\partial \nu^e_m} = \kappa_{e,s,jj'}\left\{\frac{\partial \lambda_{p,ll'}(\mathbf{r})}{\partial \nu^e_m}, \lambda_{a,hh'}(\mathbf{r})\right\}, \tag{21}$$

where $\tau_{s,jj'}\{\lambda_{p,ll'}(\mathbf{r})\}$ belong to the set of transformed parameters provided in Ref. 21.

To determine the smoothed parameters $\lambda^{\mathrm{HF}}_{e,p,jj'}$, we define an integrand $\Delta I^{\mathrm{HF}}_{e,jj'}(\mathbf{r})$ analogous to $\Delta I^{\mathrm{PT}}_{e,jj'}(\mathbf{r})$ in Eq. (17) as

$$\Delta I^{\mathrm{HF}}_{e,jj'}(\mathbf{r}) \equiv \sum_s F^*_{s,j}(\mathbf{r}) \left[\frac{\partial \tau_{s,jj'}\{\lambda^{\mathrm{HF}}_{e,p,ll'}\}}{\partial \nu^e_m} - \frac{\partial \tau_{s,jj'}\{\lambda_{p,ll'}(\mathbf{r})\}}{\partial \nu^e_m}\right] G_{s,j'}(\mathbf{r}), \tag{22}$$

One may take fields $F^*_{s,j}(\mathbf{r})$ and $G_{s,j'}(\mathbf{r})$ out of the average $\langle \Delta I^{\mathrm{HF}}_{e,jj'}(\mathbf{r})\rangle_e$. The volume integral is only applied to the variations in transformed parameters. We then proceed to set $\langle \Delta I^{\mathrm{HF}}_{e,jj'}(\mathbf{r})\rangle_e = 0$ and obtain

$$\frac{\partial}{\partial \nu^e_m}\left\langle \tau_{s,jj'}\{\lambda^{\mathrm{HF}}_{e,p,ll'}\} - \tau_{s,jj'}\{\lambda_{p,ll'}(\mathbf{r})\}\right\rangle_e = 0. \tag{23}$$

Since Eq. (23) needs to be correct for an arbitrary external variable ν^e_m, we have

$$\tau_{s,jj'}\{\lambda^{\mathrm{HF}}_{e,p,ll'}\} = \langle \tau_{s,jj'}\{\lambda_{p,ll'}(\mathbf{r})\}\rangle_e. \tag{24}$$

Equation. (24) represents a set of nonlinear equations for smoothed parameters $\lambda^{\mathrm{HF}}_{e,p,ll'}$, which can be calculated self-consistently. The detail is shown in Ref. 21.

4. RESULTS AND DISCUSSION

In this section we calculate the eigenenergies and the envelope functions $\psi^{(n,k_z)}_j(\boldsymbol{\rho})$ for semiconductor circular QWRs. The numerical errors in eigenenergies E_{n,k_z} based on the PT and HF smoothing schemes will be studied.

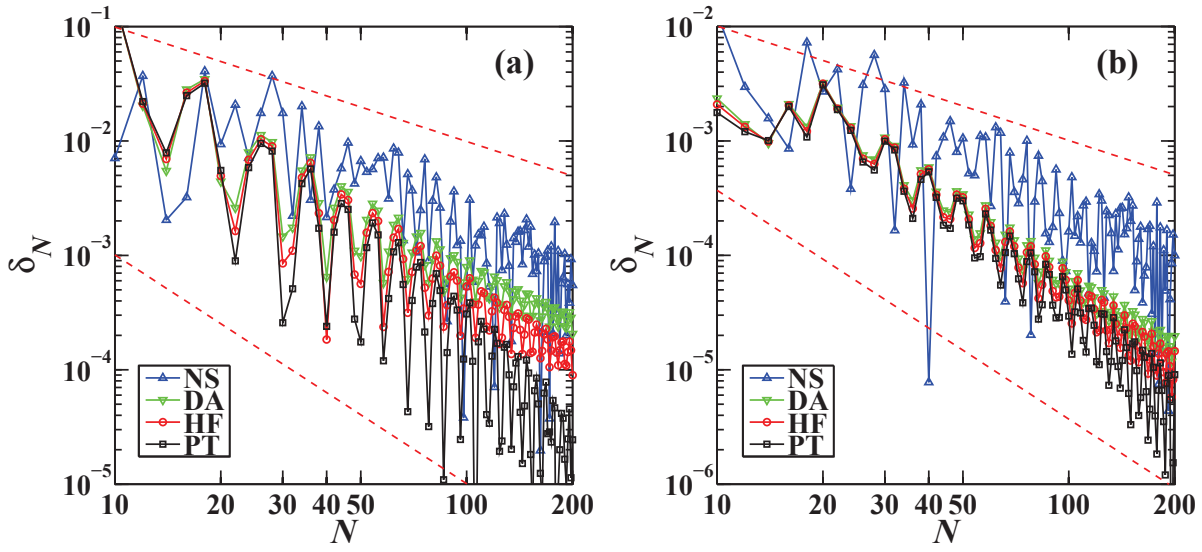

Figure 2. The relative errors δ_N as a function of the pixel number N for the (a) bound valence state with the highest energy at $k_z = 0$ nm^{-1}, and (b) bound conduction state with lowest energy at $k_z = 0.5$ nm^{-1} for the $Ga_{0.18}In_{0.82}As_{0.4}P_{0.6}$/InP QWR under the axial approximation. In (a) and (b), the upper and lower dashed lines in red indicate the trends of $O(N^{-1})$ and $O(N^{-2})$, respectively. For the valence state, the PT and HF smoothing schemes result in the lower relative errors than others do. For the conduction state, all but the one without smoothing show relative errors close to each other.

The material parameters in eight-band computations are listed in Table 1.[8,26] The modified Luttinger parameters γ_i $(i = 1-3)$ and parameter κ in the eight-band Hamiltonian are extracted from the Luttinger parameters $\gamma_i^{\rm L}$ $(i = 1-3)$ and $\kappa^{\rm L}$ for decoupled conduction (two-band) and valence bands (six-band) for the effective Hamiltonian.[9] The modified inverse effective mass γ_c in the conduction bands of eight-band Hamiltonians can be also extracted from the conduction-band effective mass m_c.[9] However, all values of γ_c for the materials in Table 1 are negative if they are computed in this way. Nonphysical spurious solutions are presented, in which the eigenenergies lie within the forbidden band gap, and envelope functions show rapid spatial oscillations. In order to remove this wing-band type of spurious solutions, we adopt the technique in Ref. 15 by setting $\gamma_c = 1$, which is equivalent to the neglect of remote bands. The modified optical matrix parameter E_p' which keeps the effective mass m_c invariant needs to be modified. Its expression is given as

$$E_p' = \left(\frac{m_0}{m_c} - 1\right) \frac{E_g(E_g + \Delta)}{E_g + 2\Delta/3}, \tag{25}$$

where m_0 is the free electron mass; E_g is the bandgap energy; and Δ is the spin-orbit split-off energy. The valence-band offsets in semiconductor heterojunctions are computed by $E_{v,av}$ using the model-solid theory.[8,27] Linear interpolations are used in parameter calculations of III-V compound materials except for bandgap energies which are estimated from Ref. 8. As an example, we examine compound semiconductors $Ga_{0.18}In_{0.82}As_{0.4}P_{0.6}$ which are lattice-matched to InP. The energy gaps E_g, modified Luttinger parameters γ_i $(i = 1-3)$, and κ of this compound are listed in Table 2.

The QWR is grown along the [001] (z) crystal axis, and its diameter is 8 nm. The computation domain has a region of 38×38 nm^2 divided into square elements of N by N pixels, where N is the the numbers of pixels in both the x ([100] axis) and y ([010] axis) directions. The material parameters inside boundary elements which are sliced by the circumference of the QWR are averaged based on the PT and HF smoothing schemes for the BF Hamiltonian. For comparisons, we also perform the computations without smoothing (NS, no smoothing) and with direct averages $\lambda^{\rm DA}_{p,e,jj'} \equiv \langle \lambda_{p,jj'}(\mathbf{r}) \rangle_e$ of heterogeneous material parameters inside boundary elements. The central-difference scheme of the FD method is utilized to solve the eigenvalue problem of QWRs in Eq. (9).

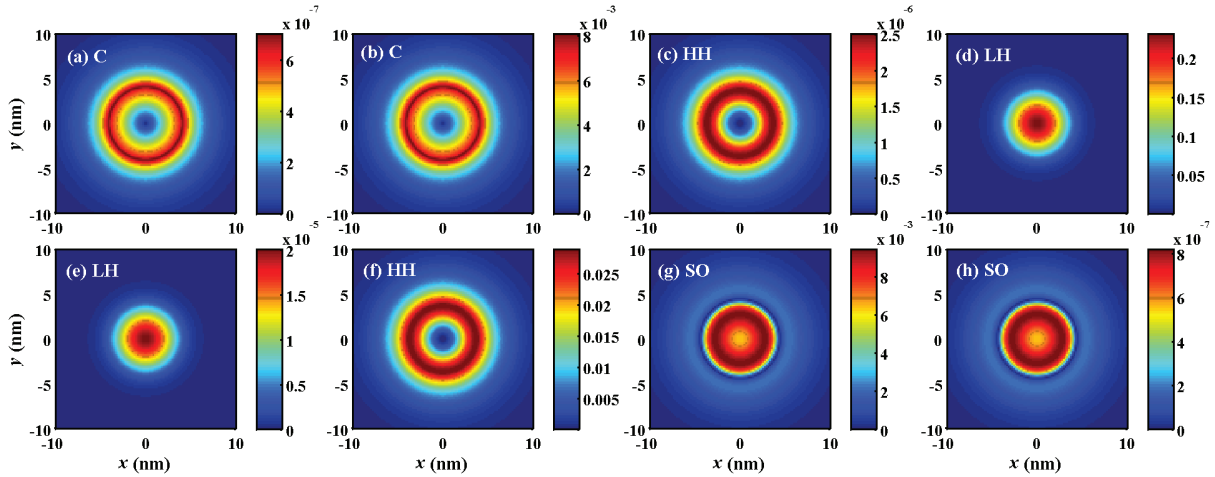

Figure 3. The numerical magnitudes $|\psi_j^{(n,k_z)}(\boldsymbol{\rho})|$ (nm^{-1}) of the valence state with the highest energy at $k_z = 0$ nm^{-1} and $N = 200$ in the PT smoothing scheme for the $Ga_{0.18}In_{0.82}As_{0.4}P_{0.6}/InP$ QWR. (a) to (h) correspond to $j = 1 - 8$. These magnitudes are nearly circularly symmetric due to the axial approximation.

With the axial approximation ($\gamma_3 - \gamma_2 \sim 0$), analytical solutions for the eigenenergies and envelope functions of eigenstates can be obtained accurately.[20,21,28] We denote the mesh-dependent eigenenergy and exact energy of a QWR state as E_N and E_{exact}, respectively. The relative error δ_N is defined as

$$\delta_N = \left| \frac{E_N - E_{\mathrm{exact}}}{E_{\mathrm{exact}}} \right|. \tag{26}$$

By plotting the behavior of δ_N with the pixel number N in the logarithmic scale, we can investigate how rapidly the numerical E_N converges to the exact value E_{exact}.

Figure 2(a) and (b) shows the relative errors δ_N for the bound valence state with the highest energy at $k_z = 0$ nm^{-1} and the counterpart of the bound conduction state with the lowest energy at $k_z = 0.5$ nm^{-1}, respectively, as a function of the pixel number N with/without smoothing for the $Ga_{0.18}In_{0.82}As_{0.4}P_{0.6}/InP$ QWR. The trends of $\mathrm{O}(N^{-1})$ and $\mathrm{O}(N^{-2})$ are also depicted for comparisons. All of the relative errors decrease as the pixel number N increases since the cross section of the QWR becomes closer to an ideal circular shape in all cases. However, the relative errors without smoothing are generally more significant. For the valence state, all relative errors present more or less oscillatory variations with the pixel number N since the mesh-dependent energy E_N tends to jump up and down around the exact energy E_{exact} with N. The relative errors in the PT, HF, and DA schemes are lower than that without smoothing. As shown in Fig. 2(a), the relative errors from the two proposed SPS methods become lower than that from the DA approach. Moreover, the PT scheme exhibit lower errors than the HF counterpart does. We denote $\delta_N \sim \mathrm{O}(N^{-m})$, in which m is the order of accuracy. The PT scheme exhibit the largest order $m > 2$ while the HF scheme has a $m \approx 2$. For the conduction state, all of the cases still show oscillatory variations on δ_N, but the trends of PT, HF, and DA schemes are close to each other. If the material parameters inside and outside the nanostructures do not deviate largely, we find the advantages of two proposed SPS schemes are more observable for valence states than for conduction ones.

Figure 3(a) to (h) shows the eight numerical magnitudes $|\psi_j^{(n,k_z)}(\boldsymbol{\rho})|$ ($j = 1 - 8$) of the valence state with the highest energy at $k_z = 0$ nm^{-1} and $N = 200$ based on the PT smoothing scheme for the $Ga_{0.18}In_{0.82}As_{0.4}P_{0.6}/InP$ QWR under the axial approximation. From (a) to (h), the envelop functions $|\psi_j^{(n,k_z)}(\boldsymbol{\rho})|$ ($j = 1 - 8$) have the components of C, C, HH, LH, LH, HH, SO, and SO in Bloch parts consecutively. All the magnitudes of envelope functions exhibit almost circularly symmetric patterns in the xy plane due to the axial approximation. The dominant magnitudes at $j = 4, 5$ show that this valence state is LH-like. However, because of the band mixing, the magnitudes of C, HH, and SO components are only lower than the LH counterpart by one order of magnitudes and hence are not negligible.

Table 3. The Bloch parts in eight-band effective Hamiltonians. The angular distributions of S, X, Y, and Z are similar to those of the s, x, y, and z orbitals in hydrogen atoms, and the two spin states are indicated as $\uparrow$ and $\downarrow$.

$\lvert u_j\rangle$	$\lvert \mathrm{j}_j, \mathrm{j}_{z,j}\rangle$	Another formulation	Type
$\lvert u_1\rangle$	$\lvert 1/2, 1/2\rangle$	$\lvert iS,\uparrow\rangle$	C
$\lvert u_2\rangle$	$\lvert 1/2, -1/2\rangle$	$\lvert iS,\downarrow\rangle$	C
$\lvert u_3\rangle$	$\lvert 3/2, 3/2\rangle$	$-\left\lvert \frac{X+iY}{\sqrt{2}},\uparrow\right\rangle$	HH
$\lvert u_4\rangle$	$\lvert 3/2, 1/2\rangle$	$-\frac{1}{\sqrt{3}}\left\lvert \frac{X+iY}{\sqrt{2}},\downarrow\right\rangle+\sqrt{\frac{2}{3}}\lvert Z,\uparrow\rangle$	LH
$\lvert u_5\rangle$	$\lvert 3/2, -1/2\rangle$	$\frac{1}{\sqrt{3}}\left\lvert \frac{X-iY}{\sqrt{2}},\uparrow\right\rangle+\sqrt{\frac{2}{3}}\lvert Z,\downarrow\rangle$	LH
$\lvert u_6\rangle$	$\lvert 3/2, -3/2\rangle$	$\left\lvert \frac{X-iY}{\sqrt{2}},\downarrow\right\rangle$	HH
$\lvert u_7\rangle$	$\lvert 1/2, 1/2\rangle$	$\sqrt{\frac{2}{3}}\left\lvert \frac{X+iY}{\sqrt{2}},\downarrow\right\rangle+\frac{1}{\sqrt{3}}\lvert Z,\uparrow\rangle$	SO
$\lvert u_8\rangle$	$\lvert 1/2, -1/2\rangle$	$\sqrt{\frac{2}{3}}\left\lvert \frac{X-iY}{\sqrt{2}},\uparrow\right\rangle-\frac{1}{\sqrt{3}}\lvert Z,\downarrow\rangle$	SO

In general, we observe that two proposed SPS procedures result in the better numerical accuracy than the unjustified DA method does due to the inclusion of the continuity of effective probability flux densities normal to interfaces. In addition, the PT scheme has the higher accuracy than the HF counterpart does. At a given level of accuracy, the fewer grid points in computation domains of nanostructures may be achieved by using SPS procedures, which could bring about the less computation time and fewer computer memories.

5. CONCLUSIONS

In summary, we have proposed two SPS schemes based on the perturbation theory and Hellmann-Feynman theorem for eight-band effective-mass Hamiltonians of semiconductor nanostructures. In these schemes, the heterogeneous material parameters in boundary elements of nanostructures are smoothed with the condition of the continuity of effective probability flux densities normal to interfaces. We implement the FD method to numerically solve the eigenenergy problem corresponding to the multiband Schrodinger's equation for circular QWRs. The eigenenergies, the relative errors versus the pixel number, and envelope functions for valence and conduction states in circular QWRs are examined under the axial approximation. Both of the proposed SPS schemes generally lead to the lower numerical errors than those with direct averages of untransformed material parameters or without smoothing. In addition, the PT approach seems to have the better accuracy than the HF procedure in inhomogeneous structures. The two developed SPS schemes may lower numerical errors and reduce the computational cost at a given level of accuracies for the modeling of semiconductor nanostructures.

APPENDIX A. MATRIX ELEMENTS OF EIGHT-BAND BURT-FOREMAN HAMILTONIAN

In eight-band Hamiltonians, the related Bloch parts $|u_j\rangle$ are denoted as $|\mathrm{j}_j, \mathrm{j}_{z,j}\rangle$ ($j = 1-8$), where j_j and $\mathrm{j}_{z,j}$ indicate the total angular momentum and magnetic quantum numbers of band j, respectively, which are similar to those of hydrogen atoms with spin-orbit coupling. The Bloch parts contain two conduction (C) bands and six valence bands, and they are listed in Table 3.[8] The six valence bands are composed of two heavy-hole (HH), two light-hole (LH), and two spin-orbit split-off (SO) bands.

The BF operator ordering is often needed for valence bands in heterostructures so that the boundary conditions across interfaces are represented correctly.[15,17,18] The matrix $\mathbf{H}[\mathbf{k}]$ of the eight-band BF Hamiltonian can

be expressed as[20,21]

$$\mathbf{H}[\mathbf{k}] = \mathbf{H}^{(\mathrm{BF})}[\mathbf{k}] + \mathbf{H}^{(\mathrm{BP})}[\boldsymbol{\varepsilon}],$$

$$\mathbf{H}^{(\mathrm{BF})}[\mathbf{k}] =$$

$$\begin{pmatrix}
E_c{+}P_{c,\mathbf{k}} & 0 & -\sqrt{3}V_+ & \sqrt{2}U & V_- & 0 & U & \sqrt{2}V_- \\
0 & E_c{+}P_{c,\mathbf{k}} & 0 & -V_+ & \sqrt{2}U & \sqrt{3}V_- & \sqrt{2}V_+ & -U \\
-\sqrt{3}V_+^{\mathrm{h.c.}} & 0 & E_v{-}P_{\mathbf{k}}{-}Q_{\mathbf{k}} & S_- & -R_{\mathbf{k}} & 0 & \frac{1}{\sqrt{2}}S_- & -\sqrt{2}R_{\mathbf{k}} \\
\sqrt{2}U^{\mathrm{h.c.}} & -V_+^{\mathrm{h.c.}} & S_-^{\mathrm{h.c.}} & E_v{-}P_{\mathbf{k}}{+}Q_{\mathbf{k}} & -C & -R_{\mathbf{k}} & \sqrt{2}Q_{\mathbf{k}} & -\sqrt{\tfrac{3}{2}}\Sigma_- \\
V_-^{\mathrm{h.c.}} & \sqrt{2}U^{\mathrm{h.c.}} & -R_{\mathbf{k}}^{\mathrm{h.c.}} & -C^{\mathrm{h.c.}} & E_v{-}P_{\mathbf{k}}^*{+}Q_{\mathbf{k}}^* & -S_+^{\mathrm{h.c.}} & -\sqrt{\tfrac{3}{2}}\Sigma_+ & -\sqrt{2}Q_{\mathbf{k}}^* \\
0 & \sqrt{3}V_-^{\mathrm{h.c.}} & 0 & -R_{\mathbf{k}}^{\mathrm{h.c.}} & -S_+ & E_v{-}P_{\mathbf{k}}^*{-}Q_{\mathbf{k}}^* & \sqrt{2}R_{\mathbf{k}}^{\mathrm{h.c.}} & \frac{1}{\sqrt{2}}S_+ \\
U^{\mathrm{h.c.}} & \sqrt{2}V_+^{\mathrm{h.c.}} & \frac{1}{\sqrt{2}}S_-^{\mathrm{h.c.}} & \sqrt{2}Q_{\mathbf{k}} & -\sqrt{\tfrac{3}{2}}\Sigma_+^{\mathrm{h.c.}} & \sqrt{2}R_{\mathbf{k}} & E_v{-}P_{\mathbf{k}}{-}\Delta & -C \\
\sqrt{2}V_-^{\mathrm{h.c.}} & -U^{\mathrm{h.c.}} & -\sqrt{2}R_{\mathbf{k}}^{\mathrm{h.c.}} & -\sqrt{\tfrac{3}{2}}\Sigma_-^{\mathrm{h.c.}} & -\sqrt{2}Q_{\mathbf{k}}^* & \frac{1}{\sqrt{2}}S_+^{\mathrm{h.c.}} & -C^{\mathrm{h.c.}} & E_v{-}P_{\mathbf{k}}^*{-}\Delta
\end{pmatrix}, \quad (27)$$

where $\mathbf{H}^{(\mathrm{BF})}[\mathbf{k}]$ consists of the $\mathbf{k}$-dependent terms related to the BF operator ordering; energies E_c and E_v on the diagonal of $\mathbf{H}^{(\mathrm{BF})}[\mathbf{k}]$ are the unstrained conduction and valence bandedge energies, respectively; Δ is the spin-orbit split-off energy; the superscript h.c. indicates the hermitian conjugate of an operator, which treats k_α ($\alpha = x, y, z$) and spatial functions noncommutable; and $\mathbf{H}^{(\mathrm{BP})}[\boldsymbol{\varepsilon}]$ is related to the strain tensor $\boldsymbol{\varepsilon}$ and corresponds to BP strain terms $P_{c,\varepsilon}$, P_ε, Q_ε, R_ε, and S_ε.[8,9] For valence bands, the terms $P_{\mathbf{k}}$, $Q_{\mathbf{k}}$, $R_{\mathbf{k}}$, $S_\pm$, $\Sigma_\pm$, and C in the BF operator ordering can be found in Refs. 20 and 21. In addition, the symmetric operator ordering are adopted for $P_{c,\mathbf{k}}$ in conduction bands and U and $V\pm$ for the coupling between conduction and valence bands, as provided in Ref. 21.

The matrix $\mathbf{H}[\mathbf{k}]$ is hermitian in the eight-band space due to the relations $P_{c,\mathbf{k}}^{\mathrm{h.c.}} = P_{c,\mathbf{k}}$, $P_{\mathbf{k}}^{\mathrm{h.c.}} = P_{\mathbf{k}}$, and $Q_{\mathbf{k}}^{\mathrm{h.c.}} = Q_{\mathbf{k}}$ (but $P_{\mathbf{k}}^* \neq P_{\mathbf{k}}$, $Q_{\mathbf{k}}^* \neq Q_{\mathbf{k}}$). For semiconductor bulks, the BF Hamiltonian $\mathbf{H}[\mathbf{k}]$ in Eq. (27) is reduced to the LK Hamiltonian[21] since the wave-vector component k_α is simply a number rather than an operator. Moreover, under the axial approximation, the matrix $R_{\mathbf{k}}$ is approximated as[8]

$$R_{\mathbf{k}} = \left(\frac{\hbar^2}{2m_0}\right)\sqrt{3}\left[-k_-\bar{\gamma}k_- + k_+\mu k_+\right] \simeq -\left(\frac{\hbar^2}{2m_0}\right)\sqrt{3}k_-\bar{\gamma}k_-, \quad (28)$$

where $\bar{\gamma} = (\gamma_3 + \gamma_2)/2$ and $\mu = (\gamma_3 - \gamma_2)/2$ are the sum and difference between $\gamma_3/2$ and $\gamma_2/2$.

ACKNOWLEDGMENTS

This work is sponsored by Research Center for Applied Sciences, Academia Sinica, Taiwan and Ministry of Science and Technology, Taiwan under Grant numbers MOST-103-2221-E-001-016 and MOST-104-2221-E-001-018.

REFERENCES

[1] Johnson, S. G., Ibanescu, M., Skorobogatiy, M. A., Weisberg, O., Joannopoulos, J. D., and Fink, Y., "Perturbation theory for Maxwell's equations with shifting material boundaries," *Phys. Rev. E* **65**(6), 066611 (2002).

[2] Farjadpour, A., Roundy, D., Rodriguez, A., Ibanescu, M., Bermel, P., Joannopoulos, J. D., Johnson, S. G., and Burr, G. W., "Improving accuracy by subpixel smoothing in the finite-difference time domain," *Opt. Lett.* **31**(20), 2972–2974 (2006).

[3] Kottke, C., Farjadpour, A., and Johnson, S. G., "Perturbation theory for anisotropic dielectric interfaces, and application to subpixel smoothing of discretized numerical methods," *Phys. Rev. E* **77**(3), 036611 (2008).

[4] Oskooi, A. F., Kottke, C., and Johnson, S. G., "Accurate finite-difference time-domain simulation of anisotropic media by subpixel smoothing," *Opt. Lett.* **34**(18), 2778–2780 (2009).

[5] Oskooi, A. F., Roundy, D., Ibanescu, M., Bermel, P., Joannopoulos, J. D., and Johnson, S. G., "MEEP: A flexible free-software package for electromagnetic simulations by the FDTD method," *Comput. Phys. Commun.* **181**(3), 687–702 (2010).

[6] Luttinger, J. M. and Kohn, W., "Motion of electrons and holes in perturbed periodic fields," *Phys. Rev.* **97**(4), 869–883 (1955).
[7] Bir, G. L. and Pikus, G. E., [*Symmetry and Strain-Induced Effects in Semiconductors*], John Wiley & Sons, New York (1974).
[8] Chuang, S. L., [*Physics of Photonic Devices*], John Wiley & Sons, Hoboken, New Jersey, second ed. (2009).
[9] Hsieh, C.-T. and Chang, S.-W., "Bound-to-continuum absorption with tunneling in type-II nanostructures: a multiband source-radiation approach," *Opt. Express* **21**(25), 30778–30795 (2013).
[10] Eissfeller, T. and Vogl, P., "Real-space multiband envelope-function approach without spurious solutions," *Phys. Rev. B* **84**(19), 195122 (2011).
[11] White, S. R. and Sham, L. J., "Electronic properties of flat-band semiconductor heterostructures," *Phys. Rev. Lett.* **47**(12), 879–882 (1981).
[12] Cartoixa, X., Ting, D. Z.-Y., and McGill, T. C., "Numerical spurious solutions in the effective mass approximation," *J. Appl. Phys.* **93**(7), 3974–3981 (2003).
[13] Kolokolov, K. I., Li, J., and Ning, C. Z., "$\mathbf{k}\cdot\mathbf{p}$ Hamiltonian without spurious-state solutions," *Phys. Rev. B* **68**(16), 161308 (2003).
[14] Veprek, R. G., Steiger, S., and Witzigmann, B., "Ellipticity and the spurious solution problem of $\mathbf{k}\cdot\mathbf{p}$ envelope equations," *Phys. Rev. B* **76**(16), 165320 (2007).
[15] Ehrhardt, M. and Koprucki, T., [*Multi-Band Efective Mass Approximations: Advanced Mathematical Models and Numerical Techniques*], Lecture Notes in Computational Science and Engineering 94, Springer (2014).
[16] Burt, M. G., "The justification for applying the effective-mass approximation to microstructures," *J. Phys.: Condens. Matter* **4**(32), 6651–6690 (1992).
[17] Foreman, B. A., "Effective-mass Hamiltonian and boundary conditions for the valence bands of semiconductor microstructures," *Phys. Rev. B* **48**(7), 4964–4967 (1993).
[18] Foreman, B. A., "Elimination of spurious solutions from eight-band $\mathbf{k}\cdot\mathbf{p}$ theory," *Phys. Rev. B* **56**(20), R12748–R12751 (1997).
[19] Lassen, B., Lew Yan Voon, L. C., Willatzen, M., and Melnik, R., "Exact envelope-function theory versus symmetrized Hamiltonian for quantum wires: a comparison," *Solid State Commun.* **132**(34), 141–149 (2004).
[20] Lew Yan Voon, L. C. and Willatzen, M., [*The* $\mathbf{k}\cdot\mathbf{p}$ *Method: Electronic Properties of Semiconductors*], Springer, Berlin (2009).
[21] Hsieh, C.-T., Hsieh, T.-H., and Chang, S.-W., "Improving accuracy using subpixel smoothing for multiband effective-mass Hamiltonians of semiconductor nanostructures." Comput. Phys. Commun., in press (2016). http://dx.doi.org/10.1016/j.cpc.2015.12.018.
[22] Chang, C.-S. and Chuang, S. L., "Modeling of strained quantum-well lasers with spin-orbit coupling," *IEEE J. Sel. Topics Quantum Electron.* **1**(2), 218–229 (1995).
[23] Chuang, S. L. and Chang, C. S., "A band-structure model of strained quantum-well wurtzite semiconductors," *Semicond. Sci. Technol.* **12**(3), 252–263 (1997).
[24] Chao, C. Y.-P. and Chuang, S. L., "Spin-orbit-coupling effects on the valence-band structure of strained semiconductor quantum wells," *Phys. Rev. B* **46**(7), 4110–4122 (1992).
[25] Cohen-Tannoudji, C., Din, B., and Laloe, F., [*Quantum Mechanics*], Hermann, Paris (1977).
[26] Lawaetz, P., "Valence-band parameters in cubic semiconductors," *Phys. Rev. B* **4**(10), 3460–3467 (1971).
[27] Van de Walle, C. G., "Band lineups and deformation potentials in the model-solid theory," *Phys. Rev. B* **39**(3), 1871–1883 (1989).
[28] Sercel, P. C. and Vahala, K. J., "Analytical formalism for determining quantum-wire and quantum-dot band structure in the multiband envelope-function approximation," *Phys. Rev. B* **42**(6), 3690–3710 (1990).